Reaction Kinetics, Mechanisms and Catalysis
https://doi.org/10.1007/s11144-021-01963-4

Photocatalytic degradation of methylene blue using sprayed Mg diluted ZnO heterostructure thin films photocatalysts

Sabrina Roguai[1,2] · Abdelkader Djelloul[1,2]

Received: 28 October 2020 / Accepted: 7 March 2021

Abstract
The thin layers of ZnOx%/MgO [x = 30, 40 and 50 at%], were prepared by the spray pyrolysis method on glass substrates at 450 °C, then tested for methyl blue (MB) degradation under visible irradiations. The ZnOx%/MgO [x = 30,40 and 50 at%] thin films were analysed by X-ray diffraction (XRD), scanning electron microscopy (SEM), UV–Vis spectroscopy and Mott-Schottky analysis. X-ray diffraction analysis revealed that the layers have a polycrystalline nature of hexagonal (wurtzite) and cubic structure. Microstructures the films were also analyzed using scanning electron. The films show a radical change in the surface morphology in accordance with the XRD results. The above analyses confirm the co-existence of a mixture of the wurtzite (ZnO) structure and cubic phase of MgO. The use of these mixed layers in the photo degradation of MB gave satisfactory results. Indeed, the photocatalytic tests showed the efficiency of Mg diluted ZnO films with the best yield in the case of 50% diluted ZO films. It was confirmed that the ZnO50%/MgO had a profound effect on reduction of band gap and photocatalytic performances.

Keywords ZnOx%/MgO thin films · Structural · Microstructural and optical properties · Photocatalysis

Introduction

Oxides semiconductor in the form of thin-film, and in particular zinc oxide (ZnO), have been the subject of a great deal of research work. The development of these materials is linked to their interesting physical properties. ZnO is a semiconductor exhibiting an

✉ Sabrina Roguai
rog.sabrina@yahoo.fr

[1] LASPI2A Laboratoire des Structures, Propriétés et Interactions Inter Atomiques, Université Abbes Laghrour, 40000 Khenchela, Algeria

[2] Science of Matter, Abbes Laghrour University, Khenchela, Algeria

Published online: 16 March 2021

attractive electrical and optical properties. The importance of its exciton binding energy (60 meV), and the width of its forbidden band (3.37 eV), make it a good candidate for applications in different technological sectors, such as the production of transparent electrodes, gas detection, photocatalysis, and ultraviolet detectors or laser diode emitting in blue or ultra violet, [1, 2], recent works are studying new ZnO formatting for applications as catalysts or sensors with good chemical properties. A new porous material has been obtained at low temperature in an acoustic cavitation reactor from Zn $(OH)_2$. The process is based on triggering the reaction between NH_3 and $Zn(OH)_2$ by ultrasonic activation in an aqueous medium [3].

The improvement in the properties of thin films of ZnO is commonly carried out through doping. Among the various dopants, the doping of ZnO with magnesium (Mg) to obtain the ternary thin films ZnMgO has been reported [4]. This new material indicates a wider band gap than ZnO and the potential of modulating the band gap by changing the rate of Mg, has received much attention due to its potential applications in ultraviolet optoelectronic devices [5]. These new thin films $Zn_{1-x}Mg_xO$ have emerged as one of the most important compounds in semiconductors due to their high binding energy [6] and also improved the photocatalytic yields [7–10].

Recently, different technological processes have been to deposit ZnO in thin layers [11–19]. One can mention the chemical methods, and the physical methods, whose physical properties of the material are strongly linked to the preparation methods. Among the new avenues that have been explored is the ultrasonic spray method. The advantage of this method consists of a better control of the size and distribution of the droplets, which in particular affects the homogeneity of the deposit, and therefore the quality of the layers. On the other hand, the pyrolytic spraying technique or reactive chemical spraying in liquid phase of precursors dissolved in water, derives its advantages from its simplicity, without vacuum and with local means. Furthermore, it has a low cost and also compared to other deposition methods such as PVD deposition. However, the physical and chemical properties of the thin films, thus, prepared depend on the deposition parameters such as the temperature of the substrate, the type and concentration of the precursors, the flow rate of the solution, the geometry of the device, etc. [20–22].

The objective of this work is the development of ZnOx%/MgO [x = 30, 40 and 50 at%] thin layers diluted by the technique of ultrasonic spray pyrolysis, on glass substrates. The structural, morphological, Mott-Schottky and optical characterization of the samples were performed. In addition the films were tested as catalysis for the methylene blue degradation.

The specific objective is to switch from doping to dilution in order to improve the optical properties, in particular by changing the optical gap energy range in order to enrich the catalytic properties.

Experimental part

Film preparation

The ultrasonic pyrolysis spray method is used as a main method to develop ZnOx%/MgO [x = 30, 40 and 50 at%] thin layers [20–22]. In this work, we will change the quantities of solvents, the deposition time as well as the flow rate in order to obtain very homogeneous layers. We have used the following precursors: Zinc acetate ($C_4H_6O_4Zn{\cdot}2H_2O$) (Fulka 99.9%); and magnesium acetate Mg (CH_3COO) (Fulka 99.9%); as the source material for Zn and Mg, which were dissolved in5 ml of methanol (Merck 99.5%) and 7.5 ml ethanol (Merck 99.5%) mixed with12.5 ml of deionized water (resistivity 18.2 MO cm). The solution is mixed for 1 h using a heating magnetic stirrer. Thin films were deposited onto microscope cover glass substrates ($30 \times 10 \times 1.2$ mm^3), with solution flow rate 0.25 ml/min, at temperature of 450 °C and the testimony time was fixed at 1 h.

Analysis of the semiconductor-electrolyte interface

Mott-Schottky experiment was carried out in 0.5 M Na_2SO_4 aqueous solution using a frequencie of 1 kHz at an applied potential ranging from − 1 to 0.2 V main-taining an ac amplitude of 10 mV at each of the potentials. All electrochemical experiments were carried out in a borosilicate glass cell with a three electrode configuration using a Pt counter electrode and an Hg/HgCl (SCE) reference electrode, and all potential here after reported are with respect to this reference electrode. The SC thin film of 4.75 cm^2.

Photodegradation of MB

The photochemical reactor used consists of a dark chamber, with a magnetic rod stirrer, and a beaker containing 10 ml of the colored solution. The thin layer is immersed in the MB (10 ml) solution so that the surface deposit under the fluorescence light of a lamp Philips germicide (G15T8/15 W) which emits mainly at wavelength of 254 nm, the distance between lamp and beaker was set at 7 cm. The concentration was determined, by measuring the absorbance, of the MB solution for well-defined time intervals by UV–Vis spectrophotometer.

Characterization techniques

For the structural properties X-ray diffraction was performed using X-ray diffractometer (MiniFlex600) with Cu K_α radiation, 0.15418 nm). The morphology of the films was examined by scanning electron microscopy (TESCAN_VEGA3) equipped with energy dispersive X-ray spectroscopy (EDS) for chemical analysis. The optical properties are determined by measuring the transmittance of the films using a

SpectroScan 80D spectrophotometer UV–Vis in the 190–1100 nm spectral range. Mott-Schottky) were measured by a CHI660E electro chemical workstation (CHI Instruments, Shanghai Chenhua Inc.).

Results and discussion

Crystalline structure of MZO thin film

Fig. 1 shows the typical XRD patterns of all prepared samples in the 2θ range of 10–80°. The data show the presence of phase mixtures characterized by the following peaks, related to (100) (002) (101) characteristic of the wurtzite phase of ZnO according to the map (00-036-1451) [16–18], while the peak around 2θ = 29° can be assigned to the MgO phase according to the map (00-030-0794). Therefore, no preferential orientation was observed, yet three directions, with varying intensities were detected because of the Mg content (x = 0.3, 0.4 and 0.5) which is clearly higher than the thermodynamic solubility limit (x = 0.04) [23].

The intensity of the peaks varies according to the rate of Mg in the films is due to the insertion of Mg in the ZnO network, we notice that the most intense characteristic peak of the wurtzite phase (002) at 34°, gradually decrease to a minimum intensity at a concentration of (50%), and the same chosen for the peak (100) is that this indicates that the wurtzite structure is degraded at this concentration, the fact that the position of the peak relative to the plane (002) is greater than the position of the reference peak (undoped ZnO), thus, indicating the presence of internal stresses in the material when the foreign atoms are inserted into the crystal lattice. The other part of the peak intensity of the MgO phase increases with the level of Mg in the films and takes a maximum intensity at a rate of 40%.

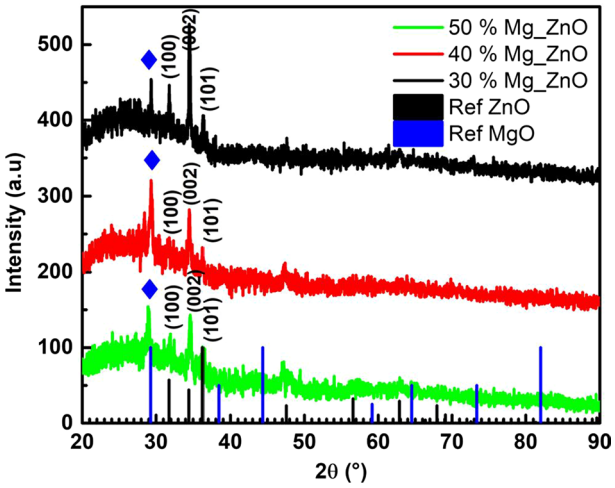

Fig. 1 XRD patterns of ZnOx%/MgO thin films (with $x = 30$, 40 and 50 at%) grown onto glass substrate by ultrasonic spray pyrolysis at 450 °C

For $Zn_{0.50}Mg_{0.50}O$ films presented two characteristic structure image of two phases ZnO (a hexagonal wurtzite structure) and MgO (a cubic structure of NaCl type) are equal, although large deviation (5.0 eV), phase cubic, metastable $Zn_{1-x}Mg_xO$ thin films can be developed with Mg incorporation greater than 50% due to the similarity in the ionic radius between Mg^{2+} (0.078) nm and Zn^{2+} (0.083) nm which allows a replacement in one or the other structure [24]. This means that the coexistence of the two phases confirms the success of the dilution of Mg in ZnO.

The microstructural parameters such as size of crystallites, the density of dislocations, deformation, residual stresses) and probability of defects stacking of the CIZO layers are calculated from the width at mid-height of the peak diffraction (002) and the peak of the MgO phase. The values obtained of the phases listed in Table 1. The size of the crystallites was calculated using the Scherrer formula [25]:

$$D = k\lambda/\beta\cos\theta \quad (1)$$

Here D is the size of the crystallites, λ the wavelength of the X-rays corresponds to the wavelength of the Kα1Cu lines (1.54056A °), θ the Bragg angle (diffraction) and β the width at mid-peak height (FWHM).

The decrease in the size of the crystallites from 35.65 to 23.84 nm of the wurtzite phase shows a degradation of the crystallinity of the thin MZO layers, this decrease is accompanied by the increase in stacking defects due to the presence of the phase of MgO, which is due to the increase in specific surface.

There is an increase in the lattice parameter then decreases with the Mg content which promotes the incorporation of the Mg particles into the ZnO network. Since the ionic radius of Mg^{2+} (0.078 nm) is close to that of Zn^{2+} (0.083 nm), inclusions of Mg should cause tangible structural changes, accompanied by a decrease in the residual stress with a negative sign indicating a compression of the structure which confirms the birth of new phase (MgO).

Surface morphology of MZO thin films

Fig. 2a–c show the top view SEM images of the MZO thin layers obtained on glass substrates by polarysis spray. In these figures, the surface of the MZO thin films are completely covered by aggregates. For $Zn_{0.70}Mg_{0.30}O$ films, it is characterized by the presence of grains in the form of nano-dots and nanotubes (nanopetals) distributed over the entire surface of the substrate. While, in the case of the $Zn_{0.60}Mg_{0.40}O$ and $Zn_{0.50}Mg_{0.50}O$ layers it is well illustrated that the surface is made of aggregates between grains in the form of nanoderms, between them other morphology of the MgO phase which appears in the form of black pores through these nano-grains. These increase with the level of Mg which explains by the difference between the ionic rays Zn^{2+}(0.083 nm) and Mg^{2+}(0.078 nm) and which confirms the insertion of Mg into the ZnO network which induces a stress causing pores in the thin film leading to increase with the rate of dilution [26]. It is important to note that the porosity of the films increases the surface accessibility of the material, which is suitable for catalytic applications as will be shown hereafter.

Table 1 X-ray diffraction data (2θ, FWHM, cell parameters 'a' and 'c',average crystallite size (D) and ε of different ZnOx%/MgO thin films

$Zn_1-_xMg_xO$ ''Nominal''Cu content (at.)	Phase ZnO						Phase MgO			
	2θ (°) value (002)	FWHM (β) (°)	a = b	c	Average crystal size (D) (nm)	ε(10^{-3})	Average crystal size (D) (nm)	Strain ε(10^{-3})	FWHM (β) (°)	2θ (°)
$Zn_{0.70}Mg_{0.30}O$	34.54	0.23	3.246	5.186	35.65	− 3.8797	26.749	− 1.3115	0.3208	29.32
$Zn_{0.60}Mg_{0\cdot40}O$	34.52	0.31	3.255	5.190	26.36	− 3.1691	19.52	− 1.4754	0.4357	29.32
$Zn_{0.50}Mg_{0.50}O$	34.62	0.34	3.243	5.175	23.84	− 6.0116	16.149	1.0.820	0.5310	28.96

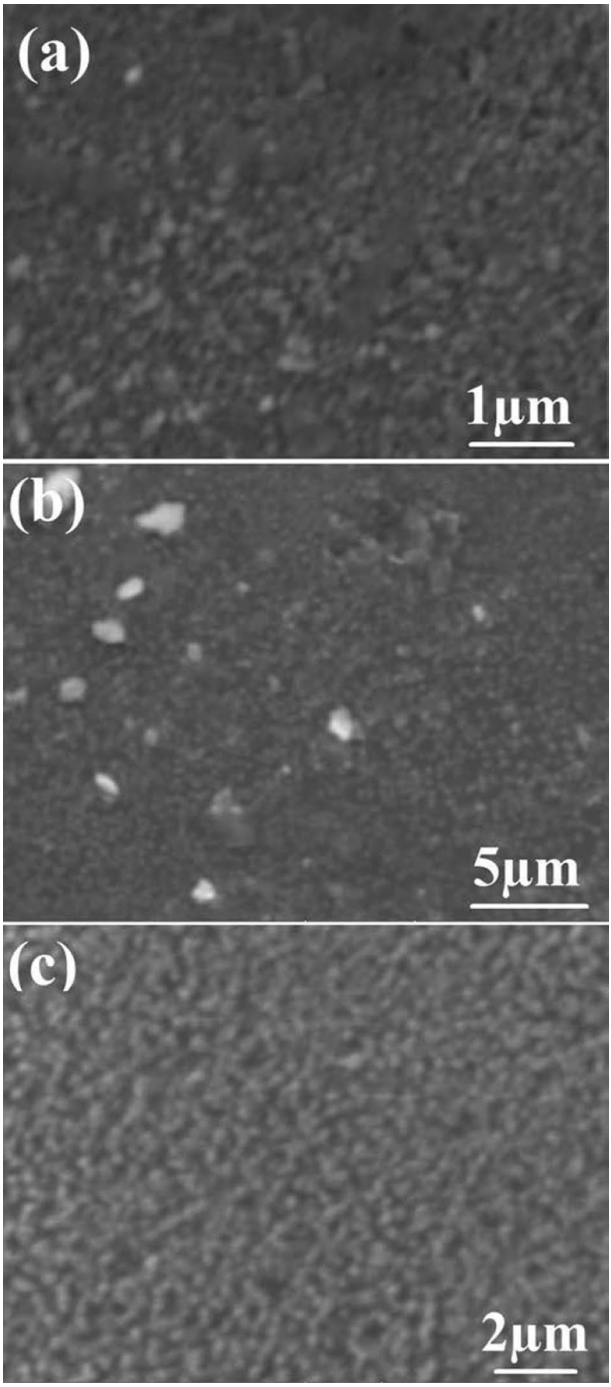

Fig. 2 SEM images of **a**–**c** ZnOx%/MgO thin films. The images **a**, **b** and **c** correspond to the Mg atomic content of 30%, 40% and 50%

Chemical composition of MZO thin films

The chemical compositions of ZnOx%/MgO [x = 30, 40, 50 at%] were determined from EDS analysis. The elemental analysis spectrum represented in Fig. 3, clearly indicates the presence of the emission lines of zinc, oxygen and magnesium. However, two additional emission lines that are attributed to silicon and calcium were also observed. The presence of this chemical element originates from the glass substrates, and the high intensity of these two peaks explained by the low thickness of the thin films [20–22].

Optical properties of MZO thin films

Fig. 4 shows the transmission spectra of MZO thin films as a function of wavelength in the range 190–1100 nm.

The appearance of all the transmission spectra measured in our samples is the same. In the visible region, the samples exhibit an average T transmission varying between 76 and 78% over a wide wavelength range from 400 to 1100 nm, which gives MZO films the character of thin transparent layers that can be used as optical windows for solar cells. The dispersion parameters of the films were evaluated using a single-effective-oscillator fit, proposed by Wemple et al. [20–22, 27]. The solid line in Fig. 4 correspond to the curve fitting and the symbols represent the experimental data, the experimental data are listed in Table 2.

All the films show sharp cut-off at the UV region together with uniform transmittance within the visible spectrum. This can be explained by the incorporation of Mg^{2+} in ZnO because of the assemblage between their ionic rays, which due to the increase in the values of the optical gap energy, this cut in the UV region is accompanied with a good transmission which corresponding to the change in

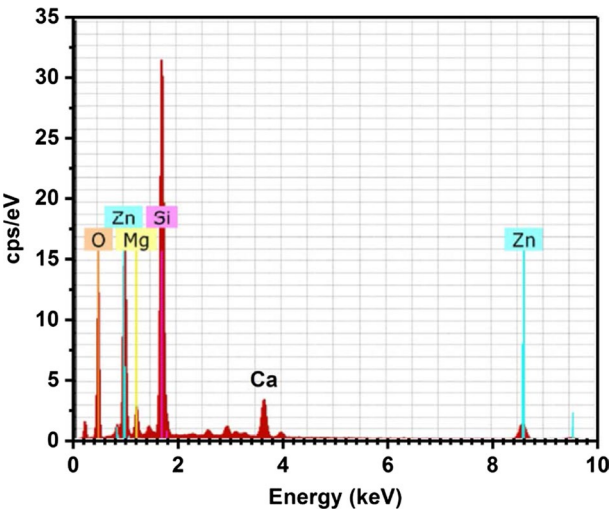

Fig. 3 Example of EDS spectrum recorded for $Zn_{0.70}Mg_{0.30}O$ thin films

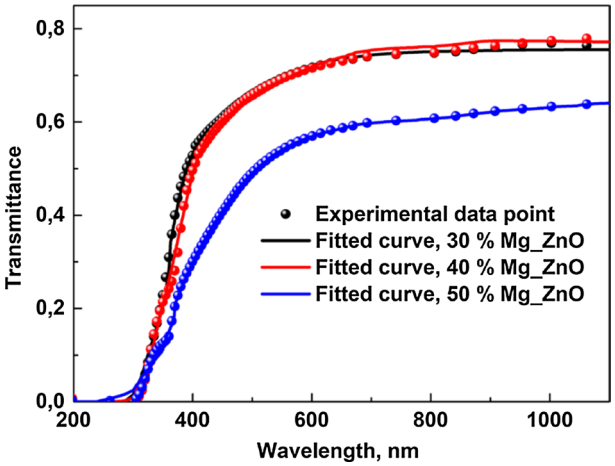

Fig. 4 Transmission spectra of ZnOx%/MgO thin films deposited on glass substrate at 450 °C. Measured (full circles) and calculated (solid lines) transmittance spectra of films

Table 2 Dispersion parameters of the ZnOx%/MgO thin films extracted by fitting the experimental data

Samples	Thickness (nm)	Eg (eV) ZnO	Eg (eV) MgO	n at 598 nm	n_∞	P
30%Mg_ZnO	196	3.62	3.84	1.67	1.55	0.2508
40%Mg_ZnO	204	3.28	3.82	1.72	1.61	0.2079
50%Mg_ZnO	219	3.23	3.84	1.58	1.46	0.3320

crystal structure. These results confirm the coexistence of two-phase crystal mixture in a good agreement with XRD and SEM analyses [28, 29].

We notice that the gap energy of the thin films ZnOx%/MgO [x = 30, 40.50 at%] for the wurtzite phase of ZnO are at equal or slightly higher values (3.62 eV, 3.28 eV, 3.23 eV), these values decrease with the decrease of the Mg content in the film. In addition, these values are much smaller in comparison to those of the optical gap of pure ZnO under the same conditions (3.25 eV) [20–22]. Indeed, this is due to the insertion of Mg^{2+} into ZnO, which is responsible for the discovery of a systematic blue change in the band gap suggests that Mg^{2+} has been correctly incorporated into the wurtzite ZnO lattice. [30]

For the MgO phase that appears, the values of the optical gap energy is a little lower than that of pure MgO produced by pyrolysis spray of 5.25 eV [31], these results may be due to the degree of non-stoichiometry of the deposited layers, which may be due to the difference of atomic interaction phenomena associated with the lattice coming into play due to the crystalline nature with the presence of oxygen vacancies and zinc interstitials. This induces a change in the electronic structure of surfaces leading to a reduction in the ionic gap and in turn its total band gap [32]. On the other hand, in the bulk, the thermodynamic limit solid

solubility of MgO in ZnO is stated to be about 4% [33]. The limit solid solubility of MgO in ZnO for thin films has been stated to be about 33 mol% when deposited using the pulsed laser deposition (PLD) technique [34], 25% when deposited using the sol–gel spin-coating technique [35], and 43% when deposited using the molecular beam epitaxy (MBE) technique [36]. And 21% as ultrasonic spray pyrolysis in the same condition [4]

The increase in optical gap energy values of MZO is explained by the Burstein-Moss phenomenon [37], which demonstrates that the donor electrons occupy the states at the bottom of the conduction band, and the Fermi level shifts towards the conduction band in the heavily doped semiconductor (in our case diluted) requires more energy resulting in an increase in the band gap [25, 37]. Therefore, confirms that there is an interaction between the two structures.

Fig. 5 presents the calculated refractive indices [20] of ZnOx%/MgO films. The values of the refractive index is a little lower compared to that of pure ZnO 1.77 [20–22], the refractive index is more sensitive to the structural defect and its decrease confirms the existence of structural defects which indicates a share the success of dilution of ZnO by Mg.

The porosity P is calculated from optical constants using the Lorentz–Lorenz equation [20]:

$$P = 1 - \left[\left(n_{film}^2 - 1\right)\left(n_{bulk}^2 + 2\right) / \left(n_{film}^2 + 2\right)\left(n_{bulk}^2 - 1\right)\right] \quad (2)$$

Here the value of n_{film} represents the refractive indices of porous ZnOx%/MgO films at 598 nm and n_{bulk} represents the refractive indices of ZnO bulk which is 1.996 at same wavelength, presented in Table 2, the values e the porosity is greater than that of pure ZnO synthesized under the same conditions at a value of P = 0.1659 [20], which is explained by the change of the crystal structure. This increase leads to the increase of the surface d 'adsorption [38]. We notice that the

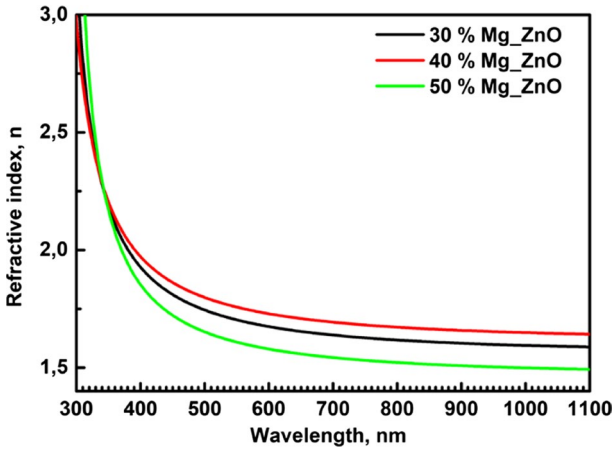

Fig. 5 Refractive index of ZnOx%/MgO thin films Refractive deposited onto glass substrate at 450 °C

films of $Zn_{0.50}Mg_{0.50}O$ take a maximum value in comparison with the other percentage in a good agreement with DRX and SEM results.

When ZnO is doped or diluted with a metal, the optical gap is directly affected, inducing the possibility of disappearance of the borders of the valence (Ev) and conduction (Ec) band. This generates the formation of states located at the end of the band at the borders of the forbidden band limited by the valence band and the conduction band. This difference expresses the disorder in a material known as Urbach energy.

In our case, we observed that the gap energy of diluted ZnO is greater than that of pure ZnO [20–22]. This has been attributed to the disorder generated by the defects in the ZnO matrix. In order to confirm this hypothesis, the Urbach energy was calculated. According to Urbach's law [39], the expression of the absorption coefficient (α) is given by the formula:

$$\ln(\alpha) = \ln(\alpha 0) + (h\nu / E_{\mathrm{Urb}}) \tag{3}$$

Here E_{Urb} is the energy of Urbach in eV and hν is the energy of the photon in eV. E_{Urb} is defined by plotting the logarithm of the absorption coefficient, and then by taking the inverse of the slope of the linear part of the plotted curve.

Fig. 6, shows the determination of the Urbach energy by extrapolation for the different types of samples developed, as well as the following variation the level of Mg. It was found that the more the dilution rate increases, the more the values of Urbach's energy increase. Therefore, the disorder structural increases. This pace remains the same for all MZOs, except for $Zn_{0.50}Mg_{0.50}O$, where the energy value of Urbach increases slightly reaching the value of 898.86 meV, so this structure presents greater disorder compared to other MZO (40 and 50 at%) [40–42].

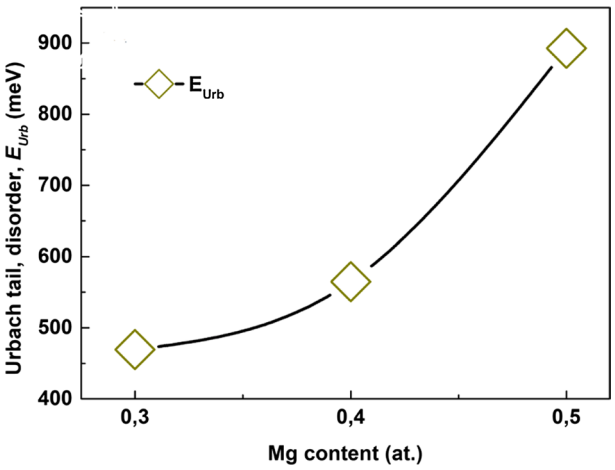

Fig. 6 **a** Plot of ln (α) vs energy to evaluate the Urbach energy ZnOx%/MgO thin films, **b** variation of Urbach energy as a function Mg diluted concentration in the films

Mott-Schottky (MS) analysis

In order to gain insights into the intrinsic electronic properties of photoanode such as flat band potential (V_{fb}) and carrier concentration (N_D), Mott-Schottky (MS) curves were recorded as shown in Fig. 7. These curves were analysed by measuring the capacitance at the electrode/electrolyte interface as a function of applied potential using the following Eq. (4) [43].

$$\frac{1}{C^2} = \frac{2}{\epsilon s \epsilon_0 A^2 e N_D}\left(V - V_{fb} - \frac{K_B T}{e}\right) \tag{4}$$

Here C is the interfacial capacitance, ϵs is the dielectric constant of the semiconductor, ϵ_0 is the permittivity of free space, e is the electronic charge, N_D is the donor density, V is the applied potential, V_{fb} is the flat band potential, k_B is the Boltzmann's constant and T is the absolute temperature. The flat band potential of the semiconductor—electrolyte interface can be obtained from the intercept on the potential axis where as the slope of the straight line is inversely related to the carrier concentration, N_D ($Slope = \frac{2}{\epsilon s \epsilon_0 A^2 e N_D}$). The positive slope of the M-S plots of ZnOx%/MgO (x = 30, 40, 50 at%), as shown in Fig. 7, confirms the n-type semiconductivity of the material and the estimated flat band potentials were -0.325 ± 0.001 V, -0.352 ± 0.001 V and -0.134 ± 0.001 V. The donor density of the ZnOx%/MgO (x = 30, 40, 50 at%) semiconductors as calculated from the slope of the M-S plots using the dielectric constant (ϵs) as 8.5, is found to be of the order of 9.27×10^{16} cm^{-3}, 7.23×10^{16} cm^{-3} and 2.16×10^{16} cm^{-3}, we notice that the values of N_D decreased with the rate of Mg and the low value of N_D for 50%Mg/ZnO can interpret the improvement of the catalytic properties at this rate. The energy band diagram for

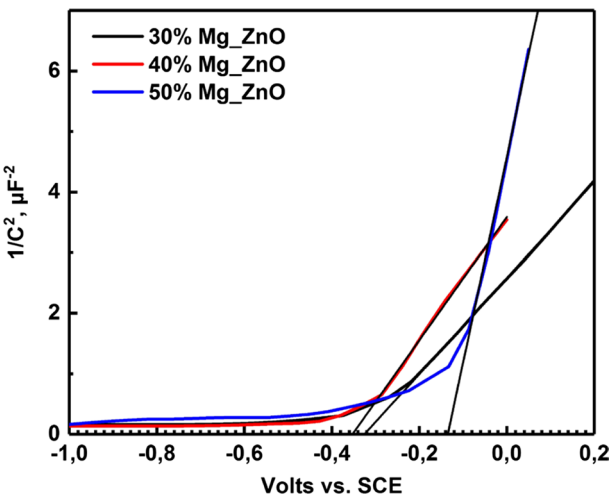

Fig. 7 Mott-Schottky plots of ZnOx%/MgO (x = 30, 40, 50 at%) films in 0.5 M Na_2SO_4 aqueous solution in dark condition. Plots were recorded at 1 kHz with an ac amplitude of 10 mV at each potential

ZnOx%/MgO (x = 30, 40, 50 at%) has been presented in Fig. 8 showing the conduction band (CB) position at −0.325 V, −0.352 Vand −0.134 Vy and that of the valence band (VB) at +3.295 V, +2.928 V and +3.096 V when measured at pH 9 working solution.

The Fermi energy (E_F) level of ZnOx%/MgO (x = 30, 40, 50 at%) was estimated from the flat band potential obtained from the Mott-Schottky analysis. The offset between the E_F level and the conduction band (E_{CB}) could be estimated according to equation below

$$E_{CB} - E_F = \frac{K.T}{e} ln \frac{N_C}{N_D} \tag{5}$$

Here k, T, and N_C are Boltzmann constant, temperature, and the effective density states at the bottom of the conduction band. The N_C could be calculated from equation below

$$N_C = 2\left(\frac{2.\prod .m^*.K.T}{h^2}\right)^{\frac{3}{2}} \tag{6}$$

Here m* and h are the effective electron mass and Planck constant. The effective electron mass of 0.27 m_o are used for calculating the N_C of doped ZnO in the ZnOx%/MgO (x = 30, 40, 50 at%) The band gaps obtained from the Tauc plots (the $(a.h.v)^2$ versus (h.v) curve) were used to calculate the E_{CB} and E_{VB} for doped ZnO in the ZnOx%/MgO (x = 30, 40, 50 at%). The Fermi energy (E_F) values calculated for ZnOx%/MgO (x = 30, 40, 50 at%) were estimated at 0.094 eV, 0.100 eV and 0.131 eV.

Photocatalytic activity of MZO thin films

In this part of the study, the photocatalytic measurements are carried out under UV in the presence of diluted samples (30% Mg_ZnO, 40% Mg_ZnO and 50%

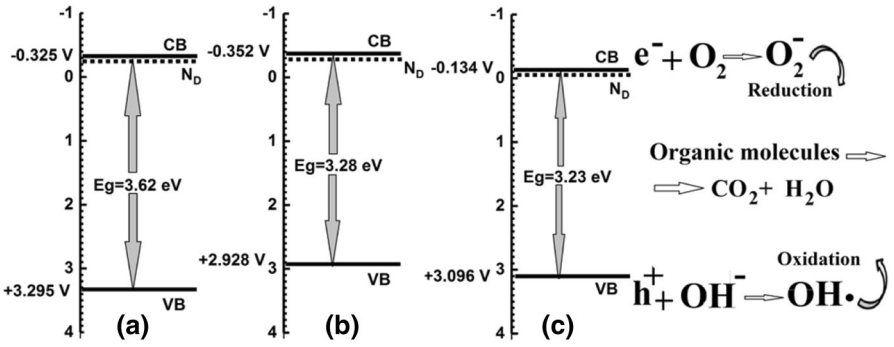

Fig. 8 Schematic showing the band diagrams of a-c ZnOx%/MgO (x = 30, 40, 50 at%) semiconductor. The Schematic a–c correspond to the Mg atomic content of 30%, 40% and 50%

Mg_ZnO), used as photocatalysis for methylene blue (MB) degradation. The photocatalytic activities are presented in Fig. 9.

The UV–Visible spectra of an MB solution obtained, characterized by two absorption bands located at approximately 614 and 664 nm is assigned to the sulfur–nitrogen conjugated system [44, 45]. From this figure, we notice a decrease in the main band with time of contact. Absorption varies from photocatalyst to photocatalyst. The maximum absorption value of MB in all spectra is 1.6 and over time is reduced indicating that methylene blue has been photo degraded.

MB decomposes continuously during the entire irradiation time for all MZO thin films. In the case of $Zn_{0.5}Mg_{0.50}O$, after 90 min of irradiation, we notice a total degradation (100%) which indicates that the best degradation is obtained at this concentration, compared to the other thin layers (30%, 40%). The absorbance of MB undergoes a large decrease during UV illumination, indicating the degradation and dissociation of MB into H_2O and CO_2.

Fig. 10 shows the kinetics of the degradation reaction of methylene blue in solution, and he calculated kinetic parameters of MB degradation are shown in Table 3, according to the following equation (7) [46].

$$A = X * \exp(-k * t) + E \tag{7}$$

While the unit of (pseudo-) order rate constant k is the inverse of the unit of time used (min^{-1}), X is the amplitude of the process, E is the endpoint, both of them have the same units as the measured quantity A.

One can see that the degradation of our dye perfectly follows a pseudo first order kinetics. While the k values for remaining thin layers were 30%Mg_ZnO (0.0028 min^{-1}), 40%Mg_ZnO (0.0049 min^{-1}), 50%Mg_ZnO (0.0051 min^{-1}). The highest k value of 50%Mg_ZnO thin films verified that the effect of Mg which

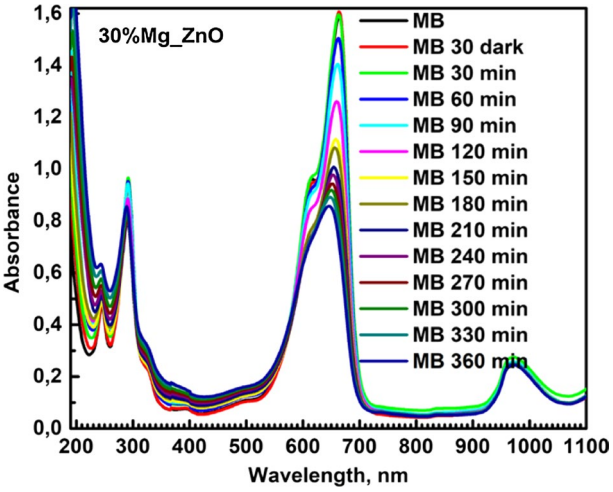

Fig. 9 The effect of $Zn_{0.70}Mg_{0.30}O$ thin film on the absorption spectra of MB solution (10 ml, 8×10^{-2} M) for different reaction time under UV light illumination

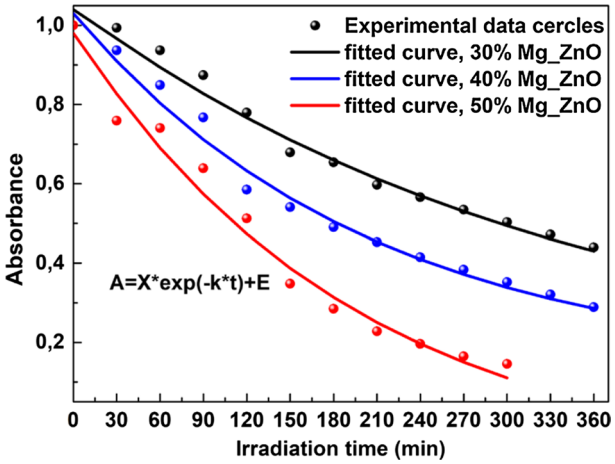

Fig. 10 Degradation kinetics of MB aqueous solutions by ZnOx%/MgO thin films [with x = 30, 40 and 50 at%] without UV light illumination. The films were prepared by using different spray pyrolysis. The photocatalytic process at UV-light follows first-order kinetics according to the equation A = X*exp(−k*t) + E, (circles) Experimental data circles and (solid lines) fitted curve (solid lines). Here A0 is the initial absorbance of the dye solution, A(t) is the absorbance at time t, and k is the rate constant of photocatalysis

improved the separation efficiency of photoinduced charge carriers and optical absorption in the visible region is the reason for increased photocatalytic activity.

Mechanism for the photocatalytic degradation of ZnO and MZO thin films

When the UV light illuminates ZnO, there is a displacement of an electron on the conduction band (e_{CB}^-) and the formation of a gap, called a hole (h_{VB}^+) in the valence band. The electron can thus participate in reduction reactions (photo-reduction) and the hole in oxidation reactions (photo-oxidation). The hole can oxidize a water molecule adsorbed on the surface of the photocatalyst to form a highly reactive hydroxyl radical and the electron can reduce an oxygen molecule adsorbed and formed a superoxide radical capable of participating in turn in oxidation reactions [29, 46]. The flat band potentials of ZnOx%/MgO (x = 30, 40, 50 at%) semiconductors were found to be -0.325 ± 0.001 V, -0.352 ± 0.001 V and -0.134 ± 0.001 V. It is apparent that the flat band potentials findings support our photocatalytic performances. And, the ZnO50%/MgO thin films had the high flat band potentials The redox potential of the photo-generated holes (−0.134 V) is high enough to drive the MB oxidation reaction ($MB \rightarrow MB+$, $E^o = +0.01$ V, in pH 7 condition), and the material exhibits excellent photoelectrochemical oxidation behavior.

The improvement in the photocatalytic performance of ZnO diluted with Mg can be attributed to a number of factors interpreting the photocatalytic efficiency of the thin films of $Zn_{0.50}Mg_{0.50}O$ compared to the two thin films $Zn_{0.70}Mg_{0.30}O$ and $Zn_{0.60}Mg_{0.40}O$:

Table 3 Pseudo-first-order kinetic parameters of MB degradation

Samples	Value			Standard deviation			R^2
	K (min^{-1})	X	E	K (min^{-1})	X	E	
$Zn_{0.70}Mg_{0.30}O$	0.0028	0.9501	0.0958	0.0008	0.1564	0.1675	0.9828
$Zn_{0.60}Mg_{0.40}O$	0.0049	0.9016	0.1317	0.0007	0.05718	0.6488	0.9871
$Zn_{0.50}Mg_{0.50}O$	0.0051	1.1147	-0.1282	0.0012	0.1252	0.1396	0.9784

Crystal structure

The photocatalytic efficiency of the catalyst varies considerably depending on its crystalline structure and in our case the structure depends on the concentration of Mg which well illustrates the formation of two phases. Therefore a change in the crystal structure which affects several parameters, The mobility of the charges shouted in the matrix of the ZnO semiconductor under the impact of photons, the size of the grains, the specific surface, the OH content of the surface, the adsorption of the species to be decomposed, the adsorption of UV photons are the parameters whose effect and play a key role on the photocatalytic yield [47], which is improved at a rate of 50% or the real coexistence of the two crystal structures can be considered with the same percentage of exitance.

The effect of morphology

The spherical structure of our layers can induce porosity and further increases the contact surface of pollutants thus the photocatalytic activity [38]. In addition, we can produce hollow spherical particles which create an internal reflection of light allowing to absorb a maximum of photons. The presence of pores due to the insertion of Mg improves the trapping of charges at the surface of the catalyst. The increase in performance is certainly due to an improvement in separation of photogenerated charge carriers. This improvement thus generates a reduction in the rate of recombination of the electron pairs. [48] and also emerges that the photocatalytic efficiencies are influenced by the concentration, the efficiency of $Zn_{0.50}Mg_{0.50}O$ is 1.35 times greater than that of $Zn_{0.70}Mg_{0.30}O$ and $Zn_{0.60}Mg_{0.40}O$.

The effect of the optical gap

For these reactions to occur, the hole must have a fairly positive potential and the electron must have a fairly negative potential. The capacity of a photocatalyst to produce these reactions and, therefore, directly linked to the width and the position of its forbidden band is the potential of the valence and conduction bands. The optical results showed that the dilution with Mg leads to obtaining two optical gape and at the same time increases the values of the forbidden band causing a higher redox potential of the pairs of electrons/photo-generated holes, which considerably increases the catalytic efficiency of MZO films [48].

Conclusion

During this study, we developed by spray pyrolysis, thin films of ZnOx%/MgO [x = 30,40, and 50 at%] deposited on glass substrates at 450 °C. We have also studied the influence of the Mg on structural microstructural, optical, and photocatalytic properties of MZO thin films.

Magnesium dilution was found to introduce pores on the surface of the films and deteriorate the crystallinity movies with mixture structure wurtzite and cubic (ZnO + MgO). The transmission spectra of MZO thin films indicate that the films is transparent in the visible and opaque in the UV. The optical bandgap calculation of films increases with increasing dilution concentration with Mg. The photo catalytic test on methylene blue shows the dilution efficiency with 50% MB degradation dilluted MZO layers increase the efficiency photocatalytic which confirmed by the Mott-Schottky analysis.

Aknowledgements The authors would like to thank the National Project Research (PNR) and LASPI^{2}A Laboratory of Khenchela University (Algeria) for their financial support of this research project.

References

1. Alnuaimi MM, Rauf MA, Ashraf SS (2007) Comparative decoloration study of Neutral Red by different oxidative processes. Dyes Pigm 72:367–371
2. Mantilla A, Tzompantzi F, Fernández JL, Góngora JD, Mendoza G, Gómez R (2009) Photodegradation of 2, 4–dichlorophenoxyacetic acid using ZnAlFe layered double hydroxides as photocatalysts. Catal Today 148:119–123
3. Rubin Thor R, Calvert Jack G, Rankin George T, Mac-Nevin W (1953) Photochemical synthesis of hydrogen peroxide at zinc oxide surfaces. J Am Chem 75:2850–2853
4. Hoggas K, Nouveau C, Djelloul A, Bououdina M (2015) Structural, microstructural, and optical properties of $Zn_{1-x}Mg_xO$ thin films grown onto glass substrate by ultrasonic spray pyrolysis. Appl Phys A 120:745–755
5. Zhang X, Min Li X, Lai Chen T, Ming Bian J, Yun Zhang C (2005) Structural and optical properties of Zn1-xMgxO thin films deposited by ultrasonic spray pyrolysis. Thin Solid Films 492:248–252
6. Etacheri V, Roshan R, Kumar V (2012) Mg–doped ZnO nanoparticles for efficient sunlight–driven photocatalysis. ACS Appl Mater Interfaces 4:2717–2725
7. Abed C, Bouzidi C, Elhouichet H et al (2015) Mg doping induced high structural quality of solgel ZnO nanocrystals: application in photocatalysis. Appl Surf Sci 349:855–863
8. Shan FK, Kim BI, Liu GX et al (2004) Blueshift of near band edge emission in Mg doped ZnO thin films and aging. J Appl Phys 95:4772
9. Lu X, Liu Z, Zhu Y et al (2011) Sonochemical synthesis and photocatalytic property of zinc oxide nanoparticles doped with magnesium(II). Mater Res Bull 46:1638–1641
10. Etacheri V, Roshan R, Kumar V (2012) Mg-doped ZnO nanoparticles for efficient sunlight-driven photocatalysis. ACS Appl Mater Interfaces 4:2717–2725
11. Caglar Y, Aksoy S, Ilican S, Caglar M (2009) Crystalline structure and morphological properties of undoped and Sn doped ZnO thin films. Superlattices Microstruct 46:469–475
12. Peng LP, Fang L, Yang XF, Li YJ, Huang QL, Wu F, Kong CY (2009) Effect of annealing temperature on the structure and optical properties of In–doped ZnO thin films. J Alloys Compds 484:575–579
13. Wang XC, Chen XM, Yang BH (2009) Microstructure and optical properties of polycrystalline ZnO films sputtered under different oxygen flow rates. J Alloys Compd 488:232–237

14. Zhu G, Shulin G, Zhu S, Huang S, Ran G, Ye J, Zheng Y (2012) Optimization study of metal–organic chemical vapor deposition of ZnO on sapphire substrate. J Cryst Growth 349:6
15. Aksay S, Caglar Y, Ilican S, Caglar M (2011) Sol–gel derived zinc oxide films: effect of deposition parameters on structure, microstructure and photoluminescence properties. Superlattices Microstruct 50:470–479
16. Jiao SJ, Lu YM, Shen DZ, Zhang ZZ, Li BH, Zheng ZhH, Yao B, Zhang JY, Zhao D, Fan XW (2007) Donor–acceptor pair luminescence of nitrogen doping p–type ZnO by plasma–assisted molecular beam epitaxy. J Lumines 122:368–370
17. Savchuk AI, Fediv VI, Savchuk SA, Perrone A (2005) Growth and characterization of ZnMnO thin films. Superlattices Microstruct 38:421–427
18. Tsay ChY, Fan KSh, Lei ChM (2012) Synthesis and characterization of sol–gel derived gallium–doped zinc oxide thin films. J Alloys Compds 512:216–222
19. Roguai S, Djelloul A, Nouveau C, Souier T, Dakhel AA, Bououdina M (2014) Structure, microstructure and determination of optical constants from transmittance data of co–doped Zn0.90Co0.05M0.05O (M = Al, Cu, Cd, Na) films. J Alloys Compd 599:150–158
20. Roguai S, Djelloul A (2019) Synthesis and evaluation of the structural, microstructural, optical and magnetic properties of Zn1−*x*Co*x*O thin films grown onto glass substrate by ultrasonic spray pyrolysis. Appl Phys A 125:816
21. Roguai S, Djelloul A (2020) A structural and optical properties of Cu–doped ZnO films prepared by spray pyrolysis. Appl Phys A 126:122
22. Segnit ER, Holland AE (1965) The System MgO-ZnO-SiO_2. Ceram Soc 48:412
23. Choopun S, Vispute RD, Yang W, Sharma RP, Venkatesan T, Shen H (2002) Realization of band gap above 5.0 eV in metastable cubic- phase MgxZn1−xOMgxZn1−xO alloy films. ApplPhysLett 80:1529
24. Anandhi R, Mohan R, Swaminathan K, Ravichandran K (2012) Influence of aging time of the starting solution on the physical properties of fluorine doped zinc oxide films deposited by a simplified spray pyrolysis technique. Superlattices Microstruct 51:680–689
25. Zheng G, Shang W, Xu L et al (2015) Enhanced photocatalytic activity of ZnO thin films deriving from a porous structure. Mater Lett 150:1–4
26. Wemple SH, DiDomenico M (1971) Behavior of the electronic dielectric constant in covalent and ionic materials. Phys Rev B 3:1338–2135
27. Xin M (2019) Optical properties of nanostructured ZnO: Eu film by sol–gel method. Surf Eng 35:947–953
28. Sernelius BE, Berggren KF, Jin ZC et al (1988) Band–gap tailoring of ZnO by means of heavy Al doping. Phys Rev B 37:10244
29. Boshta M, Abou-Helal MO, Ghoneim D, Mohsen NA, Zaghlool RA (2010) The photocatalytic activity of sprayed $Zn_{1-x}Mg_xO$ thin films. Surf Coat Technol 205:271–274
30. Moses Ezhil Raj A, Nehru LC, Jayachandran M, Sanjeeviraja C (2007) Spray pyrolysis deposition and characterization of highly (100) oriented magnesium oxide thin films. Cryst Res Technol 42:867–875
31. Raj A, Nehru LC, Jayachandran M, Sanjeeviraja C (2007) Spray pyrolysis deposition and characterization of highly (100) oriented magnesium oxide thin films. Cryst Res Technol 42:867
32. Bhattacharya P, Das RR, Katiyar RS (2004) Comparative study of Mg doped ZnO and multilayer ZnO/MgO thin films. Thin Solid Films 447:564
33. Ohtomo A, Kawasaki M, Koida T, Masabuchi K, Koinuma H, Sakurai Y, Yoshida Y, Yasuda T, Segawa Y (1998) MgxZn1-xO as a II–VI widegap semiconductor alloy. Appl Phys Lett 72:2466
34. Singh A, Vij A, Kumar D, Khanna PK, Kumar M, Gautam S, Chae KH (2013) Investigation of phase segregation in sol–gel derived ZnMgO thin films. Semicond Sci Technol 28:025004
35. Koike K, Hama K, Nakashima I, Takada GY, Ogata KI, Sasa S, Inoue M, Yano M (2005) Molecular beam epitaxial growth of wide bandgap ZnMgO alloy films on (111)- oriented Si substrate toward UV-detector applications. J Cryst Growth 278:288
36. Zhu Q, Lu J, Wang Y et al (2016) Burstein-Moss effect behind Au surface plasmon enhanced intrinsic emission of ZnO microdisks. Sci Rep 6:36194
37. Rai RC (2013) Analysis of the Urbach tails in absorption spectra of undoped ZnO thin films. J Appl Phys 113:153508
38. Urbach F (1953) The long–wavelength edge of photographic sensitivity and electronic absorption of solids. APS J Phys Rev 92:1324–1326

39. Kawano Y, Kodani Y, Chantana J et al (2016) Effects of Na and secondary phases on physical properties of SnS thin film after sulfurization process. Jpn J Appl Phys 55:092301
40. Hjiria M, Aida MS, Lemine OM et al (2019) Study of defects in Li–doped ZnO thin films. Mater Sci Semicond Process 89:149–153
41. Saha D, Das AK, Ajimsha RS et al (2013) Effect of disorder on carrier transport in ZnO thin films grown by atomic layer deposition at different temperatures. J Appl Phys 114:043703
42. Bhattacharya C, Lee HC, Bard AJ (2013) Rapid screening by scanning elec-trochemical microscopy (SECM) of dopants for Bi2WO6improved photo-catalytic water oxidation with Zn doping. J Phys Chem C 117:9633
43. Zhao ZF, Zhou XY, Zhang WM (1990) Instrument analysis, 1st edn. Higher Education Press, Beijing
44. Sharma K, Vyas RK, Dalai AK (2017) Thermodynamic and kinetic studies of methylene blue degradation using reactive adsorption and its comparison with adsorption. J Chem Eng Data 62:3651–3662
45. Lente G (2015) Deterministic kinetics in chemistry and systems biology. Springer, New York, pp 52–58
46. Singh S, Thiyagarajan P, Kant KM, Anita D, Thirupathiah S, Rama N, Tiwari B, Kottaisamy M, Rao MSR (2007) Structure, microstructure and physical properties of ZnO based materials in various forms: bulk, thin film and nano. J Phys D Appl Phys 40:6312–6327
47. Peng Y, Qin S, Wang W et al (2013) Fabrication of porous Cd–doped ZnO nanorods with enhanced photocatalytic activity and stability. CrystEngComm 15:6518–6525
48. Wang Y, Zhao X, Duan L et al (2015) Structure, luminescence and photocatalytic activity of Mg-doped ZnO nanoparticles prepared by auto combustion method. Mater Sci Semicond Process 29:372–379